Research Paper
Computational Methods for Differential Equations
http://cmde.tabrizu.ac.ir
Vol. *, No. *, *, pp. 1-18
DOI:10.22034/cmde.2026.68119.3282

On the multigrid method in modeling tumor growth with estimation and reduction of discretization error

Jesika Maganin[1,*], Marcio Augusto Villela Pinto[1], Neyva Maria Lopes Romeiro[2], and Sebastião Romero Franco[3]

[1]Graduate Program in Numerical Methods in Engineering, Federal University of Paraná, Curitiba, Brazil.

[2]Department of Mathematics, State University of Londrina, Londrina, Paraná, Brazil.

[3]Department of Mathematics, State University of the Central West, Irati, Paraná, Brazil.

Abstract

In this work, we investigate the efficient solution of a two-dimensional model of avascular tumor growth, described by a transient system of four partial differential equations, two of which are nonlinear. The main contribution of this study lies in the strategic combination of the multigrid method with the standard Repeated Richardson Extrapolation (RRE) technique, aiming to reduce discretization error and enhance computational performance. The system was discretized using finite differences: central differences for the spatial terms and the Crank-Nicolson scheme for the temporal discretization. Linearization was performed via Taylor series expansion, and the resulting linear system was solved using the red-black Gauss-Seidel iterative method accelerated by multigrid. Code verification was initially carried out using a manufactured solution with Dirichlet boundary conditions, allowing accurate error analysis. Subsequently, a realistic setting was simulated, using an initial condition that characterizes tumor morphology. The results show that the combination of the multigrid method and the RRE technique significantly reduced computational time while maintaining a consistently low average convergence factor and producing highly accurate and reliable solutions, demonstrating the potential of the proposed multigrid-RRE approach for the accurate and efficient numerical simulation of avascular tumor growth models.

Keywords. Numerical simulation, Finite difference method, Biomathematics, Multigrid, Repetead Richardson extrapolation.

1991 Mathematics Subject Classification. 65M06, 65M55, 65N22.

1. Introduction

In Engineering, there is a growing need to understand natural phenomena, particularly those involving fluid dynamics, in which Biomathematics plays a fundamental role. Many of these phenomena are described by mathematical equations and models, facilitating the understanding of interactions in biological systems [1, 4, 42, 48]. However, real-world problems often lack known analytical solutions, requiring computational approaches to generate approximate results.

In this context, Computational Fluid Dynamics (CFD) emerges as a field aimed at simulating thermofluid dynamic phenomena, seeking to reduce the need for experimental procedures and explore phenomena that are difficult to study experimentally. The mathematical models used in CFD demand numerical methods capable of providing accurate, reliable, and efficient solutions [15]. However, discretizing such problems leads to large-scale systems of equations, which traditional numerical methods often struggle to solve efficiently.

To achieve efficient solutions and significantly improve convergence in solving systems of equations for a wide range of problems, including elliptic, parabolic, and hyperbolic equations, the multigrid method is employed [5, 49]. This method uses a grid hierarchy to address the full spectrum of error frequencies, resulting in faster convergence. Its versatility and effectiveness contribute to the efficient solution of linear systems across several fields, such as fluid simulation, structural analysis, biomedicine, and other areas of computational modeling [43]. Recent works focusing

Received: 12 July 2025; Accepted: 01 September 2026.
∗ Corresponding author. Email: jesikamaganin@ufpr.br.

on efficient numerical methods using the multigrid technique include Al-Mahdawi et al. [2], Habibi et al. [17], Malacarne et al. [23], Ramezani et al. [28], de Oliveira et al. [31], Pinto et al. [32], de la Riva et al. [36], Santiago et al. [43].

Beyond solving linear systems efficiently, it is essential that numerical solutions be accurate, as numerical errors can compromise the reliability of computational simulations. Controlling or minimizing these errors is critical, and estimation techniques are applied for this purpose. Discretization error is one of the main sources of numerical error, and techniques such as mesh refinement and extrapolation are commonly used to mitigate it [25]. Richardson Extrapolation (RE) [11, 25, 38] is a well-established and computationally inexpensive method in this context. When applied recursively, it is known as Repeated Richardson Extrapolation (RRE) [38], which can enhance its effectiveness. Studies exploring the RRE technique include Foltran et al. [14], Leduc [20], Marchi et al. [25], Merga and Chemeda [27], Rodrigues et al. [39], da Silva et al. [45, 46].

It is worth noting that second-order numerical methods, although widely used due to their simplicity and stability, require highly refined meshes to achieve satisfactory accuracy, which can increase computational costs. However, the multigrid method proves effective in accelerating convergence even on such refined meshes, making it a valuable tool in this context.

This study proposes the integration of the multigrid method with the RRE technique to solve a tumor growth model described by partial differential equations (PDEs), aiming to combine computational efficiency with solution accuracy. The distinguishing feature of this approach lies in the strategic combination of these techniques for a physical problem of biological interest, which is still underexplored in the context of numerical verification. Furthermore, the RRE technique employed here can be readily adapted to higher-order schemes, as demonstrated by da Silva et al. [45], who combined RRE with fourth-order schemes for the Poisson equation.

The main objective of this work is to analyze discretization errors and calibrate error estimators. A complementary article, focused on the biological analysis of the model, including parameter study and variable behavior, is currently under development.

The proposed model consists of a system of PDEs describing the interactions among tumor cells, extracellular matrix, matrix-degrading enzymes, and endogenous inhibitors [3, 18, 21]. The system was discretized using the finite difference method on uniform meshes, applying central differences (CDS) for spatial terms and the Crank-Nicolson scheme for temporal discretization. Nonlinear terms were linearized using Taylor series expansion [6]. The resulting linear systems were solved using the red-black Gauss-Seidel iterative method, accelerated with a geometric multigrid method employing a V-cycle. The RRE technique was applied to estimate and reduce discretization error.

We performed numerical experiments in two scenarios: initially with a problem having a known analytical solution, to verify the accuracy and robustness of the method; and subsequently with a realistic problem without a known solution, to assess the reliability of the final results. The outcomes demonstrate the effectiveness of the proposed integrated approach.

In recent years, several mathematical models of tumor invasion have been proposed and refined [3, 7–9, 12, 16, 18, 19, 47]. However, issues related to numerical verification and the computational efficiency of these models remain underexplored in the literature. Some studies employ the multigrid method to accelerate the convergence of numerical solutions in tumor models, such as Ng and Frieboes [29], Wise et al. [50, 51], but do not adopt systematic techniques for discretization error estimation and reduction, such as RRE. Although the mathematical model considered in this work is governed by time-dependent equations, the discrete spatial problems arising at each time step exhibit an elliptic character. This property makes the multigrid method especially attractive, as it is widely regarded as one of the most efficient techniques for the solution of elliptic partial differential equations. Therefore, employing multigrid throughout the temporal integration process can substantially reduce computational cost without compromising accuracy. Nevertheless, the use of multigrid combined with systematic numerical verification techniques remains relatively unexplored in the tumor growth modeling literature.

Within this context, the present work seeks to solve a system of equations modeling tumor growth more efficiently, robustly, and accurately than conventional methods, while maintaining low computational cost.

The paper is organized as follows: Section 2 presents the mathematical and numerical model. Section 3 introduces the basic concepts of the multigrid method and the error analysis. In Section 4, we discuss the results of numerical

experiments for two cases: first, a test using an analytical solution; and second, a test involving a realistic problem. Finally, Section 5 presents the conclusions.

2. Material and methods

2.1. **Mathematical model.** Developed in Kolev and Zubik-Kowal [18], the mathematical model describes the growth of generic solid tumors in the avascular stage, aiming to analyze interactions between the tumor and surrounding tissue. The model comprises four time-dependent partial differential equations (PDEs) for the variables: cancer cell density, extracellular matrix density (ECM), concentration of matrix-degrading enzymes (MDE), and concentration of tissue inhibitors of metalloproteinases (TIMP) (known as endogenous inhibitor), denoted as n, f, m, and u, respectively, and is given by

$$\frac{\partial n}{\partial t} = \underbrace{d_n \Delta n}_{\text{diffusion}} - \underbrace{\gamma \nabla \cdot (n \nabla f)}_{\text{haptotaxis}} + \underbrace{\mu_1 n(1-n-f)}_{\text{proliferation}}, \tag{2.1}$$

$$\frac{\partial f}{\partial t} = - \underbrace{\eta m f}_{\text{degradation}} + \underbrace{\mu_2 f(1-n-f)}_{\text{renewal}}, \tag{2.2}$$

$$\frac{\partial m}{\partial t} = \underbrace{d_m \Delta m}_{\text{diffusion}} + \underbrace{\alpha n}_{\text{production}} - \underbrace{\theta u m}_{\text{neutralization}} - \underbrace{\beta m}_{\text{decay}}, \tag{2.3}$$

$$\frac{\partial u}{\partial t} = \underbrace{d_u \Delta u}_{\text{diffusion}} + \underbrace{\xi f}_{\text{production inhibitor}} - \underbrace{\theta u m}_{\text{neutralization}} - \underbrace{\rho u}_{\text{decay}}, \tag{2.4}$$

in the spatial domain $\Omega \subseteq \mathbb{R}^2$. The Δ, ∇, and $\nabla\cdot$ represent, respectively, the Laplacian, the gradient and the divergence operator, and the time interval (t) considered is $(0, t_f)$. Initial and boundary conditions will be presented in section 4.1 and 4.2.

The model Eqs. (2.1)-(2.4) establish that the migration of tumor cells creates spatial gradients that direct the migration of invasive cells through a mechanism called haptotaxis, represented by γ. The diffusion constants of the cancer cell density, matrix-degrading enzymes (MDE), and inhibitor are given, respectively, by d_n, d_m, and d_u. The proliferation rate of tumor cells and the growth rate of the ECM are represented by μ_1 and μ_2, while η, α, θ, β, ξ, and ρ are positive constants. The values of all these physical parameters can be seen in Section 4 and Kolev and Zubik-Kowal [18], López et al. [21], Maganin et al. [22].

2.2. **Numerical model.** The system of partial differential equations given by Eqs. (2.1)-(2.4) is discretized using the Crank–Nicolson scheme for time integration [10] and the Finite Difference Method (FDM) with second-order central differences for spatial discretization. The spatial step sizes in the x- and y-directions are assumed equal, that is, $h_x = h_y = h$. The temporal step size is defined by $\tau = \frac{t_f}{N_t - 1}$, where t_f denotes the final simulation time and N_t is the total number of time levels. The resulting nonlinear algebraic system is subsequently linearized using a first-order Taylor expansion [44].

Let $N_{i,j}^k$, $F_{i,j}^k$, $M_{i,j}^k$, and $U_{i,j}^k$ denote the finite difference approximations to the continuous solutions $n(x_i, y_j, t_k)$, $f(x_i, y_j, t_k)$, $m(x_i, y_j, t_k)$, and $u(x_i, y_j, t_k)$, respectively. The computational grid is defined by $x_i = ih$, $y_j = jh$, and $t_k = k\tau$, where the indices i and j identify the spatial grid points, and k denotes the time level.

2.2.1. *Discretization of the cancer cell density equation.* For Eq. (2.1), the Crank–Nicolson scheme is employed for temporal discretization and second-order central differences are used for spatial discretization. This yields

$$\begin{aligned} \frac{N_{i,j}^{k+1} - N_{i,j}^k}{\tau} = \frac{1}{2}\Big[& d_n \Delta_h N_{i,j}^{k+1} - \gamma \left(\nabla_h \cdot \left(N^{k+1} \nabla_h F^{k+1} \right) \right)_{i,j} + \mu_1 N_{i,j}^{k+1} - \mu_1 \left(N_{i,j}^{k+1} \right)^2 \\ & - \mu_1 N_{i,j}^{k+1} F_{i,j}^{k+1} + S n_{i,j}^{k+1} + d_n \Delta_h N_{i,j}^k - \gamma \left(\nabla_h \cdot \left(N^k \nabla_h F^k \right) \right)_{i,j} \\ & + \mu_1 N_{i,j}^k - \mu_1 \left(N_{i,j}^k \right)^2 - \mu_1 N_{i,j}^k F_{i,j}^k + S n_{i,j}^k \Big], \end{aligned} \tag{2.5}$$

where the discrete diffusion operator is approximated by

$$(\nabla_h \cdot (N\nabla_h F))_{i,j} = \frac{N_{i+1,j} - N_{i-1,j}}{2h}\frac{F_{i+1,j} - F_{i-1,j}}{2h} + N_{i,j}\frac{F_{i-1,j} - 2F_{i,j} + F_{i+1,j}}{h^2} + \frac{N_{i,j+1} - N_{i,j-1}}{2h}\frac{F_{i,j+1} - F_{i,j-1}}{2h} + N_{i,j}\frac{F_{i,j-1} - 2F_{i,j} + F_{i,j+1}}{h^2}. \tag{2.6}$$

Since Eq. (2.5) contains the nonlinear term $\left(N_{i,j}^{k+1}\right)^2$, a first-order Taylor expansion is employed to linearize the equation and obtain a linear system at each time level:

$$\left(N_{i,j}^{k+1}\right)^2 \simeq -\left(N_{i,j}^{k}\right)^2 + 2N_{i,j}^{k}N_{i,j}^{k+1}. \tag{2.7}$$

Substituting Eq. (2.7) into Eq. (2.5) and rearranging the resulting expression yields

$$a_{n5}N_{i,j}^{k+1} = a_{n1}\left(N_{i-1,j}^{k+1} + N_{i+1,j}^{k+1} + N_{i,j-1}^{k+1} + N_{i,j+1}^{k+1}\right) - \frac{1}{4}a_{n2}\left[\left(N_{i+1,j}^{k+1} - N_{i-1,j}^{k+1}\right)\left(F_{i+1,j}^{k+1} - F_{i-1,j}^{k+1}\right) + \left(N_{i,j+1}^{k+1} - N_{i,j-1}^{k+1}\right)\left(F_{i,j+1}^{k+1} - F_{i,j-1}^{k+1}\right)\right] + Fn_{i,j}^{k+1}, \tag{2.8}$$

where the auxiliary coefficients and source term are defined as

$$a_{pa} = \frac{1}{\tau}, \qquad a_{n1} = \frac{d_n}{2h^2}, \qquad a_{n2} = \frac{\gamma}{2h^2}, \qquad a_{n3} = \frac{\mu_1}{2}, \qquad a_{n4} = \frac{1}{\tau} + \frac{2d_n}{h^2} - \frac{\mu_1}{2},$$

$$a_{n5} = a_{n4} + a_{n2}\left(F_{i,j-1}^{k+1} + F_{i,j+1}^{k+1} + F_{i-1,j}^{k+1} + F_{i+1,j}^{k+1} - 4F_{i,j}^{k+1}\right) + a_{n3}\left(2N_{i,j}^{k} + F_{i,j}^{k+1}\right),$$

and

$$Fn_{i,j}^{k+1} = N_{i,j}^{k}\left(a_{n3}N_{i,j}^{k} + a_{pa}\right) + \frac{d_n}{2h^2}\left(N_{i-1,j}^{k} + N_{i+1,j}^{k} + N_{i,j-1}^{k} + N_{i,j+1}^{k} - 4N_{i,j}^{k}\right) - \frac{\gamma}{8h^2}\left[\left(N_{i+1,j}^{k} - N_{i-1,j}^{k}\right)\left(F_{i+1,j}^{k} - F_{i-1,j}^{k}\right) + \left(N_{i,j+1}^{k} - N_{i,j-1}^{k}\right)\left(F_{i,j+1}^{k} - F_{i,j-1}^{k}\right) + 4N_{i,j}^{k}\left(F_{i-1,j}^{k} + F_{i+1,j}^{k} + F_{i,j-1}^{k} + F_{i,j+1}^{k} - 4F_{i,j}^{k}\right)\right] + a_{n3}\left(1 - N_{i,j}^{k} - F_{i,j}^{k}\right)N_{i,j}^{k} + \frac{1}{2}\left(Sn_{i,j}^{k} + Sn_{i,j}^{k+1}\right).$$

2.2.2. *Discretization of the extracellular matrix density equation.* For Eq. (2.2), the Crank–Nicolson scheme is employed for temporal discretization. Since no spatial derivatives are present, only the reaction terms are discretized. The nonlinear terms are then linearized using a first-order Taylor expansion, yielding

$$a_{f3}F_{i,j}^{k+1} = Ff_{i,j}^{k+1}, \tag{2.9}$$

where the auxiliary coefficients and source term are defined as

$$a_{f3} = a_{pa} + a_{f1}M_{i,j}^{k+1} + a_{f2}\left(N_{i,j}^{k+1} + 2F_{i,j}^{k} - 1\right),$$

with

$$a_{f1} = \frac{\eta}{2}, \qquad a_{f2} = \frac{\mu_2}{2},$$

and

$$Ff_{i,j}^{k+1} = a_{pa}F_{i,j}^{k} + a_{f2}\left(F_{i,j}^{k}\right)^2 - a_{f1}M_{i,j}^{k}F_{i,j}^{k} + a_{f2}F_{i,j}^{k}\left(1 - N_{i,j}^{k} - F_{i,j}^{k}\right) + \frac{1}{2}\left(Sf_{i,j}^{k+1} + Sf_{i,j}^{k}\right).$$

2.2.3. *Discretization of the matrix degrading enzymes equation.* For Eq. (2.3), the Crank–Nicolson scheme is employed for temporal discretization, while the diffusion term is approximated using the standard five-point stencil. Rearranging the resulting expression yields

$$a_{m6}M_{i,j}^{k+1} = a_{m1}\left(M_{i-1,j}^{k+1} + M_{i+1,j}^{k+1} + M_{i,j-1}^{k+1} + M_{i,j+1}^{k+1}\right) + a_{m4}N_{i,j}^{k+1} + F_{m}{}_{i,j}^{k+1} \tag{2.10}$$

where the auxiliary coefficients and source term are defined as

$$a_{m1} = \frac{d_m}{2h^2}, \qquad a_{m2} = \frac{\beta}{2}, \qquad a_{m3} = \frac{\theta}{2}, \qquad a_{m4} = \frac{\alpha}{2},$$

$$a_{m5} = \frac{1}{\tau} + \frac{2d_m}{h^2} + \frac{\beta}{2}, \qquad a_{m6} = a_{m5} + a_{m3}U_{i,j}^{k+1},$$

and

$$\begin{aligned} F_{m}{}_{i,j}^{k+1} =& a_{pa}M_{i,j}^{k} + a_{m1}\left(M_{i-1,j}^{k} + M_{i+1,j}^{k} + M_{i,j-1}^{k} + M_{i,j+1}^{k} - 4M_{i,j}^{k}\right) + a_{m4}N_{i,j}^{k} - a_{m3}U_{i,j}^{k}M_{i,j}^{k} \\ & - a_{m2}M_{i,j}^{k} + \frac{1}{2}\left(Sm_{i,j}^{k+1} + Sm_{i,j}^{k}\right). \end{aligned}$$

2.2.4. *Discretization of the tissue inhibitor of metalloproteinases equation.* For Eq. (2.4), the Crank–Nicolson scheme is employed for temporal discretization, while the diffusion term is approximated using the standard five-point stencil. Rearranging the resulting expression yields

$$a_{u5}U_{i,j}^{k+1} = a_{u1}\left(U_{i-1,j}^{k+1} + U_{i+1,j}^{k+1} + U_{i,j-1}^{k+1} + U_{i,j+1}^{k+1}\right) + a_{u3}F_{i,j}^{k+1} + Fu_{i,j}^{k+1}, \tag{2.11}$$

where the auxiliary coefficients and source term are defined as

$$a_{u1} = \frac{d_u}{2h^2}, \qquad a_{u2} = \frac{\rho}{2}, \qquad a_{u3} = \frac{\xi}{2}, \qquad a_{u4} = \frac{1}{\tau} + \frac{2d_u}{h^2} + \frac{\rho}{2}, \qquad a_{u5} = a_{u4} + a_{m3}M_{i,j}^{k+1},$$

and

$$\begin{aligned} Fu_{i,j}^{k+1} =& a_{pa}U_{i,j}^{k} + a_{u1}\left(U_{i-1,j}^{k} + U_{i+1,j}^{k} + U_{i,j-1}^{k} + U_{i,j+1}^{k} - 4U_{i,j}^{k}\right) + a_{u3}F_{i,j}^{k} - a_{m3}U_{i,j}^{k}M_{i,j}^{k} - a_{u2}U_{i,j}^{k} \\ & + \frac{1}{2}\left(Su_{i,j}^{k+1} + Su_{i,j}^{k}\right). \end{aligned}$$

The discrete equations (2.8)–(2.11) form the resulting large-scale coupled linear algebraic system. The solution of this system requires an efficient and robust numerical strategy. Therefore, a multigrid method is employed, as described in the following section.

3. Theory and calculation

3.1. **Fundamentals of the multigrid method.** The multigrid method is an advanced numerical technique used to solve linear systems resulting from the discretization of differential equations, particularly in boundary value problems. Originally proposed by Fedorenko [13], the method aims to accelerate the convergence of classical iterative solvers by employing a hierarchical grid strategy (fine and coarse).

Conventional iterative methods, such as Gauss-Seidel, exhibit good convergence rates only during the initial iterations, when error components are highly oscillatory (high-frequency Fourier modes). However, as iterations proceed and the error becomes smoother (dominated by low-frequency Fourier modes), convergence slows significantly [49].

In such cases, the multigrid method stands out as a robust and efficient approach, designed to reduce both high- and low-frequency errors. According to Briggs et al. [5], smooth error components on a fine grid appear more oscillatory when observed on coarser grids. Based on this principle, the multigrid method uses a sequence of grids with increasing coarseness, alternating smoothing steps at each level and approximating solutions on coarser grids. This process relies on restriction operators, which transfer residuals to coarser levels, and prolongation operators, which interpolate corrections back to finer grids, thereby accelerating global convergence by addressing the entire error spectrum [5, 49].

Depending on how information is gone through between grid levels, one can adopt either the Correction Scheme (CS) or the Full Approximation Scheme (FAS). As recommended by Briggs et al. [5], CS is suitable for linear problems,

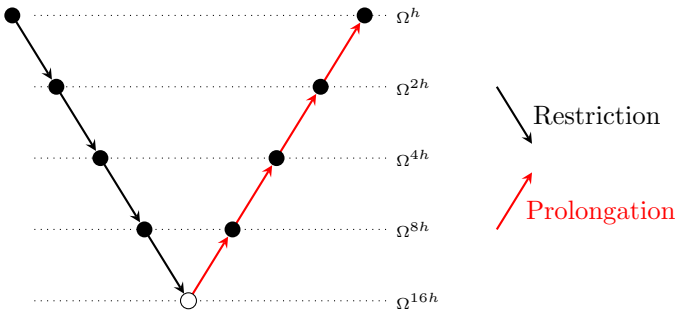

FIGURE 1. Structure of the V-cycle. The symbol • represents smoothing and the symbol ∘ represents the exact solution.

whereas FAS is more appropriate for nonlinear ones. Since the tumor model in this study was previously linearized, only the CS is employed here.

Different strategies for going through the grid hierarchy lead to various cycle types, such as the V-cycle, W-cycle, and F-cycle. In this study, we adopt the $V(\nu_1, \nu_2)$-cycle, illustrated in Figure 1, using five grid levels with standard coarsening ratio, where ν_1 and ν_2 denote the numbers of pre- and post-smoothing steps, respectively.

The V-cycle was chosen for its robustness, ease of implementation, and widespread adoption in problems governed by PDEs with features similar to the tumor model used. This choice also allowed for more direct control over convergence parameters, enabling a comparative analysis under varying spatial and temporal discretizations. Moreover, when properly configured, the V-cycle is among the most computationally efficient multigrid strategies.

In this work, we apply a decoupled, time-stepping formulation in which each equation of the system is solved independently. As each equation has elliptic structure, the multigrid V-cycle proved to be particularly efficient in accelerating convergence during each time step.

It is important to note that the main focus of this study was on evaluating the computational efficiency of the classical multigrid configuration combined with Repeated Richardson extrapolation. The investigation of alternative cycles, such as the $W-$ or $F-$cycle or cascadic multigrid, is considered a promising direction and is being explored as a future extension of this research.

Algorithm 1 is based on the $V(\nu_1, \nu_2)$-cycle for the CS scheme considering a certain grid level $l > 1$ with grid spacings $h, 2h, 4h, \ldots, 2^{l-1}h$, where $I_{2^{l-1}h}^{2^l h}$ and $I_{2^l h}^{2^{l-1}h}$ are, respectively, the restriction and prolongation operators.

Algorithm 1: MG-V-Cycle(l)

if $l = L_{max}$ *is the coarsest grid level* **then**
  Solve the system $A_l v^{(l)} = f^{(l)}$ on the coarse grid $\Omega^{2^{l-1}h}$.
  else
    Smooth ν_1 times $A_l v^{(l)} = f^{(l)}$ on the grid $\Omega^{2^{l-1}h}$.
    Calculate and restrict the residual $f^{(l+1)} = I_{2^{l-1}h}^{2^l h}(f^{(l)} - A_l v^{(l)})$.
    Solve at the next level **MG-V-Cycle(l+1)**.
    Correct using interpolation $v^{(l)} \leftarrow v^{(l)} + I_{2^l h}^{2^{l-1}h} v^{(l+1)}$.
    Smooth ν_2 times $A_l v^{(l)} = f^{(l)}$ on the grid $\Omega^{2^{l-1}h}$.
  end
end

3.2. **Error analysis.**

3.2.1. *Numerical error.* The numerical error (E) corresponds to the difference between the exact analytical solution (Φ) of a variable of interest and its numerical solution (ϕ), that is,

$$E = \Phi - \phi. \tag{3.1}$$

In general, the main sources of numerical error are: truncation errors, iteration errors, and rounding errors [24, 35]. When truncation errors are the only source of numerical error considered, meaning that iteration and rounding errors are neglected or minimized, the numerical error is called discretization error $E(\phi)$. It can be defined using the Taylor series expansion as described in [37]

$$E(\phi) = c_0 h^{p_0} + c_1 h^{p_1} + c_2 h^{p_2} + c_3 h^{p_3} + \ldots = \sum_{V=0}^{\infty} c_V h^{p_V}, \tag{3.2}$$

where the coefficients $c_V, V = 0, 1, 2, 3, \ldots$ are real numbers obtained as functions of the dependent variable of the problem and its derivatives, but independent of h. By definition, the true orders (p_V), are the exponents of h, and they are positive integers following the relationship $1 \leq p_0 < p_1 < p_2 < p_3 \ldots$. The first true order, p_0, is called the asymptotic order and is denoted by p_A.

It is possible to verify *a posteriori* whether the order of discretization error obtained by the numerical model coincides with its asymptotic order calculated *a priori*. This analysis is based on the calculation of the effective order (p_E) when the analytical solution is known; otherwise, it relies on the calculation of the apparent order (p_U). Since the main objective of this article is to analyze a realistic problem, that is, a problem whose analytical solution is not known, we will consider only the apparent order, as described by [46]

$$p_U = \frac{log\left|\dfrac{\phi_C - \phi_{SC}}{\phi_F - \phi_C}\right|}{log(q)}, \tag{3.3}$$

where ϕ_F, ϕ_C and ϕ_{SC} are the numerical solutions obtained, respectively, on the fine (h_F), coarse (h_C) and super-coarse (h_{SC}) grids, generated with a refinement ratio $q = \dfrac{h_C}{h_F} = \dfrac{h_{SC}}{h_C}$. Theoretically, the apparent order tends towards the asymptotic order with mesh refinement, i.e., $p_U \to p_A$ when $h \to 0$ [39, 45, 46].

It should be emphasized that all discretizations used in Section 2.2, both the spatial discretization by CDS and the temporal discretization by Crank-Nicolson, have asymptotic orders $p_A = 2$. Therefore, in this paper, we are dealing with methods where $p_A = 2$ globally [33, 35].

3.2.2. *Repeated Richardson Extrapolation.* The method of Repeated Richardson Extrapolation (RRE) [11, 25] is a numerical post-processing technique used to improve the accuracy of a numerical estimate, especially in iterative methods.

The main idea of RRE is to perform several iterations of a numerical method and then combine these iterations in a specific way to obtain a more accurate estimate. When using FDM, for example, this quantity obeys the true orders (p_V) of the difference equation used to approximate the derivatives of the differential equation, but it can also be based on equivalent apparent orders [46].

Considering the numerical solution of a particular variable of interest (ϕ), on G distinct grids Ω^{h_1}, Ω^{h_2}, ..., $\Omega^{h_{g-1}}$, Ω^{h_g}, ..., Ω^{h_G} generated with a refinement ratio $q = h_{g-1}/h_g$ ($g = 2, \ldots, G$), the use of the RRE with m levels of extrapolation is given by

$$\phi_{g,m} = \phi_{g,m-1} + \frac{\phi_{g,m-1} - \phi_{g-1,m-1}}{q^{p_{m-1}} - 1}, \qquad m = 1, \ldots, g-1. \tag{3.4}$$

These values can be theoretically determined *a priori* and confirmed through the concept of apparent order p_U of discretization error accuracy [14, 46],

$$(p_U)_{g,m} = \frac{log\left(\frac{\phi_{g-1,m} - \phi_{g-2,m}}{\phi_{g,m} - \phi_{g-1,m}}\right)}{log(q)}. \tag{3.5}$$

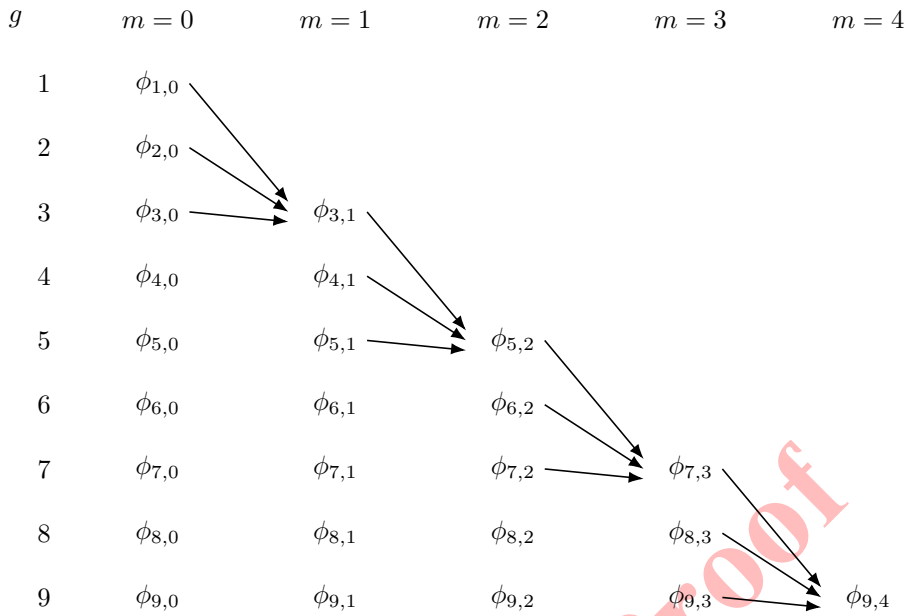

FIGURE 2. Practical scheme for the RRE of numerical solution for $g = 9$ and $m = 4$.

In Figure 2, we present the representation of RRE to facilitate the understanding of extrapolations. At least three solutions are required to perform an extrapolation in cases where the analytical solution is unknown (using p_U). The larger the values of g and m, the lower the discretization error associated with the extrapolated variable (the RRE algorithm can be consulted in da Silva et al. [45]).

3.2.3. *Estimates for the discretization error.* When the analytical solution ϕ is unknown, the discretization error cannot be calculated. Instead, the concept of uncertainty (U) is used. The uncertainty of a numerical solution is determined by the difference between the estimated analytical solution (ϕ_∞) for a variable of interest and its numerical solution (ϕ), that is,

$$U(\phi) = \phi_\infty - \phi. \tag{3.6}$$

To estimate the discretization error, Richardson's error estimator based on the apparent and asymptotic orders was used because it is widely reported in the literature, serving as a reference estimator [26]. Richardson's error estimators are given by:

$$U_{Ri}(p_U) = \frac{(\phi_F - \phi_C)}{(q^{p_U} - 1)}, \qquad U_{Ri}(p_V) = \frac{(\phi_F - \phi_C)}{(q^{p_V} - 1)}, \tag{3.7}$$

with p_U given by Eq. (3.3).

To obtain the discretization error estimate considering the use of RRE, we will use two estimators from the literature: the Corrected Richardson Estimator (pmc) and ψ^* Estimator [25, 39]. The discretization error estimate according to the Corrected Richardson Estimator is given by:

$$U_{pmc}(\phi_{g,m}) = r^{p_m} \frac{\phi_{g+1,m} - \phi_{g,m}}{q^{p_m} - 1}, \tag{3.8}$$

where r^{p_m} is a correction factor. The discretization error estimate according to the ψ^* Estimator is given by:

$$U_{\psi^*}(\phi_{g,m}) = \frac{\phi_{g,m} - \phi_{g-1,m-1}}{\psi^* - 1}, \qquad \psi^* = \psi_{g+1}; g = 2, \ldots, G-1. \tag{3.9}$$

for $g = 2, \ldots, G$, where

$$\psi^* = \begin{cases} \frac{\phi_{g,m} - \phi_{g-1,m-1}}{\phi_{g+1,m+1} - \phi_{g,m}}, & g = 2, 3, \ldots, G-1 \\ \frac{(\phi_{g-1,m-1} - \phi_{g-2,m-2})^2}{(\phi_{g,m} - \phi_{g-1,m-1})(\phi_{g-2,m-2} - \phi_{g-3,m-3})}, & g = G. \end{cases} \tag{3.10}$$

3.2.4. *Effectiveness of an error estimate.* In cases where the analytical solution Φ is not known, the quality of an estimate (U) for the numerical error (E) becomes extremely important. To evaluate the quality of the estimate, we can calibrate estimators in problems where their analytical solution is known. In this case, we can assess the effectiveness $\theta(U)$ of such estimators, which is defined as the ratio between U and E. An ideal error estimate is one where $\theta = 1$, meaning $U = E$. However, in realistic situations where $U \neq E$, the estimate is considered accurate when $\theta(U) \approx 1$ [39, 53].

4. Results and discussion

This section focuses on the verification of numerical solutions and the results obtained from the implementation of a two-dimensional tumor growth model. It is divided into two parts: in Section 4.1, the model is modified to derive an analytical solution for the purpose of code verification, using the Method of Manufactured Solutions (MMF). Following the verification of the code, in Section 4.2 we use the model with initial conditions that reflect a realistic problem.

The simulations were performed on a computer equipped with an Intel(R) Core(TM) i7-7700 3.60 GHz processor, 32 GB of RAM, and a 64-bit Windows 10 operating system. The algorithms were implemented using Microsoft Visual Studio 2022, Version 17.6.0, and Fortran Compiler 2023.1. Given the aim to investigate discretization errors and fully utilize the power of the Repeated Richardson Extrapolation (RRE), all real-type variables were defined with quadruple precision.

The use of RRE requires obtaining numerical solutions for a specific variable of interest across different meshes. In this study, the variables of interest (N, F, M and U) are evaluated at the central point of the domain at the final time step, due to the critical importance of this point for clinical analysis.

The numerical solutions were determined using 10 different levels of discretization while maintaining a constant refinement ratio $q = 2$. This implies that the spatial ($N_x = N_y$) and temporal (N_t) discretization is given by $N = N_x = N_y = N_t = 2^{nm} + 1$, with $nm = 2, \ldots, 11$, resulting in $N = 5, 9, 17, \ldots, 2049$. The solution of the system of equations, resulting from the discretization using the Finite Difference Method (FDM), is performed using a multigrid approach, employing the red-black Gauss-Seidel iterative method as the smoother. We adopted the stopping criterion $\frac{||r(it)||_\infty}{||r(0)||_\infty} \leq \varepsilon$, where $r(it)$ and $r(0)$ are the residuals at the current iteration and the initial estimate, respectively, with $\varepsilon = 10^{-8}$ as the adopted threshold. The results obtained using the multigrid method employed a $V(\nu_1, \nu_2)$ cycle with $\nu_1 = 0$ and $\nu_2 = 2$ for pre- and post-smoothing, respectively. The full weighting operator was used for restriction, bilinear interpolation for prolongation, and a standard coarsening ratio was applied.

The analysis of the apparent orders was conducted using the norm $||Eh||_\infty$. Regarding the number of points in the spatial and temporal discretizations, we have $N = 2^{nm} + 1$, where nm, represents the number of mesh levels in the x and y directions, for the multigrid method. In cases where multiple meshes are not used, this will be referred to as singlegrid in this paper.

4.1. **Numerical test with analytical solution .** To derive an analytical solution for code verification and error analysis, we employed the Method of Manufactured Solutions (MMS) [30]. This method aims to generate an exact analytical solution without considering the physical reality of the problem. An analytical function is defined and used as the dependent variable in the partial differential equation (PDE), with all its derivatives calculated analytically. The PDE is then constructed such that any additional terms that do not satisfy the original PDE are grouped into a source term. This source term is subsequently incorporated into the original PDE to fully satisfy the new PDE [34, 40].

For our case ($\Omega \subseteq \mathbb{R}^2$), we assume the initial condition given by

$$\mathbf{u}(\mathbf{x}, 0) = \sin(2\pi x) \sin(2\pi y), \tag{4.1}$$

where $\mathbf{u} = [n, f, m, u]$, $\mathbf{x} \in \Omega$, $\Omega = [0, 0.5] \times [0, 0.5]$, with $\mathbf{x} = (x, y)$. The boundary conditions are of the Dirichlet type, that is

$$\mathbf{u}(\mathbf{x_b}, t) = 0, \tag{4.2}$$

with $\mathbf{x_b} \in \partial\Omega$, $0 < t \leq t_f$.

The source terms f_n, f_f, f_m and f_u, are determined such that Eqs. (2.1)-(2.4) satisfy the analytical solution

$$\overline{\mathbf{u}}(\mathbf{x}, t) = e^t \sin(2\pi x) \sin(2\pi y), \tag{4.3}$$

$$f(\mathbf{x}, t) = e^{-t} \sin(2\pi x) \sin(2\pi y), \tag{4.4}$$

with $\overline{\mathbf{u}} = [n, m, u]$, $\mathbf{x} \in \Omega$, $0 \leq t \leq t_f$.

Thus, the source terms are given by

$$\begin{aligned} s_n(\mathbf{x}, t) = &[(((-8\gamma\pi^2 + \mu_1)\sin(2\pi y)^2 + 4\gamma\cos(2\pi y)^2\pi^2)\sin(2\pi x)^2 \\ &+ 4\gamma\cos(2\pi x)^2\pi^2\sin(2\pi y)^2)e^{-t} + (1 + 8d_n\pi^2 - \mu_1 + \mu_1 e^t A)A]e^t, \end{aligned} \tag{4.5}$$

$$s_f(\mathbf{x}, t) = (\eta + \mu_2)A^2 + (-1 - \mu_2 + \mu_2 A e^{-t})Ae^{-t}, \tag{4.6}$$

$$s_m(\mathbf{x}, t) = (1 + 8d_m\pi^2 - \alpha + \beta + \theta A e^t)Ae^t, \tag{4.7}$$

$$s_u(\mathbf{x}, t) = (1 + 8d_u\pi^2 + \rho + \theta A e^t - \xi e^{-2t})Ae^t, \tag{4.8}$$

$\mathbf{x} \in \Omega$, $0 < t \leq t_f$, with $A = \sin(2\pi x)\sin(2\pi y)$. For the verification of the code with the analytical solution, we consider $t_f = 0.25$ and the physical parameters given in Table 1, as per Kolev and Zubik-Kowal [18], López et al. [21], Maganin et al. [22]

TABLE 1. Values of the physical parameters.

Parameters	γ	d_n, d_m, d_u	μ_1	μ_2, α	η	θ	β, ρ	ξ
Values	0.01	0.001	0.2	0.1	10	0.05	0.07	0.03

Using the MMS, we will analyze the convergence and computational time (t_{CPU}) of the singlegrid and multigrid methods, employing the average convergence factor (ρ_m) and speed-up (S). Initially, we define the convergence factor (ρ), given by [49]

$$\rho(it) = \frac{||r(it)||_\infty}{||r(it-1)||_\infty}, \tag{4.9}$$

where it denotes the number of iterations in the singlegrid method or cycles in the multigrid method.

As a performance measure of the methods, we use the average convergence factor ρ_m, defined by

$$\rho_m = \sqrt[it]{\rho(1).\rho(2).\rho(3)\ldots.\rho(it)}. \tag{4.10}$$

According to Trottenberg, Oosterlee and Schuller (2001), when $\rho_m \approx 1$, it indicates a low rate of convergence, whereas $\rho_m \approx 0$, indicates a high rate of convergence for the iterative methods.

In Figure 3 we can observe the values of ρ_m for the singlegrid and multigrid methods as the mesh refinement progresses, considering the process for the 4 variables at the final time. As the mesh is refined, we observe in this figure that $\rho_m \to 1$ for the singlegrid case, as expected. For the multigrid case, we have $\rho_m \approx 0$. Therefore, we can ensure that the multigrid method exhibits good performance regardless of mesh refinement. This indicates that the method is capable of solving the problem efficiently, requiring less computational effort, even for large-scale problems.

According to Roy, Anand and Donzis [41], the computational effort of a numerical method is evaluated by analyzing the behavior of the t_{CPU} in seconds (s) as a function of the total number of unknowns in each mesh ($\mathcal{N}$), such that

$$\mathcal{N} = 4(N_x - 2)(N_y - 2)(N_t - 1), \tag{4.11}$$

where the factor 4 represents the four variables.

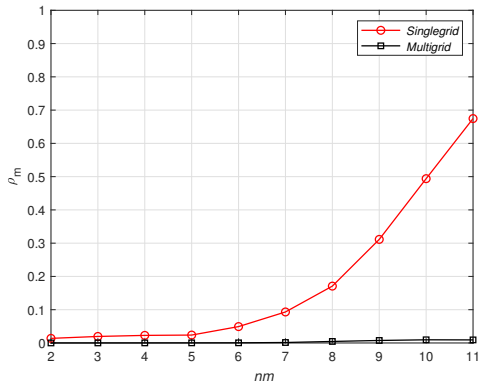

FIGURE 3. ρ_m for the singlegrid and multigrid methods.

TABLE 2. t_{CPU} and S of the singlegrid and multigrid methods.

nm	$t_{CPU}(SG)$	$t_{CPU}(MG)$	S
4	2.34E-02	1.35E-02	1.74
5	2.39E-01	2.57E-02	9.31
6	1.22E+00	1.28E-01	9.53
7	7.69E+00	8.48E-01	9.07
8	7.46E+01	5.35E+00	13.94
9	9.73E+02	5.45E+01	17.86
10	1.26E+04	5.88E+02	21.45
11	2.69E+05	4.39E+03	61.18

One way to compare the computational effort of the singlegrid (SG) and multigrid (MG) methods is by calculating the ratio between the computational time of the singlegrid ($t_{CPU}(SG)$) and multigrid ($t_{CPU}(MG)$). This ratio is known as speed-up (S), and is given by [49, 52]:

$$S = \frac{t_{CPU}(SG)}{t_{CPU}(MG)}, \tag{4.12}$$

which can be seen in Table 2.

The speed-up S represents how many times faster the multigrid method is compared to the singlegrid method. For example, for $nm = 11$, which corresponds to a spatial mesh of 2049×2049 nodes and 2049 times steps, the CPU time for the SG and MG methods to solve the four variables of interest is, 268807 s and 4393.5 s, respectively. This means the MG method is approximately 61 times faster than the SG method, as shown in Figure 4.

We observe in Figure 4 that for all evaluated numbers of unknowns, the multigrid method is always faster than the singlegrid method, and this advantage increases as $\mathcal{N}$ grows, which is a highly desirable property.

Next, to verify the code using Equation (3.5), the apparent order (p_U) of the discretization error was analyzed for the variables of interest N, F, M, and U. Based on the results shown in Figures 3 and 4, this analysis will be performed using only the multigrid method. To isolate the effect of the discretization error and examine its behavior, we must minimize or even eliminate the influence of other error sources. To achieve this, the iterative process of the simulations was terminated upon reaching rounding error.

The order p_U was evaluated for these variables of the physical problem at the central point of the domain. Using the RRE technique, as $h \to 0$, the values of p_U are expected to converge to the values of p_V at the respective extrapolation level (m). The results are presented in Figure 5.

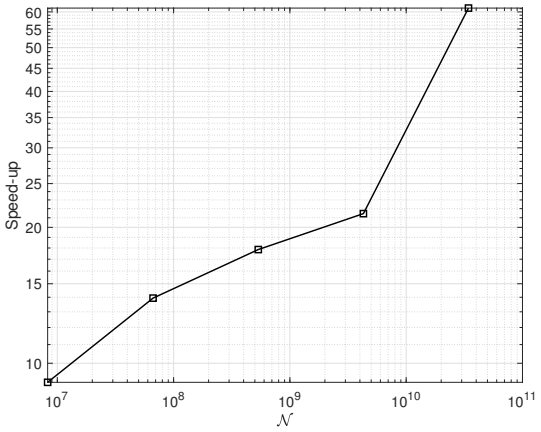

FIGURE 4. Speed-up (S) of the singlegrid and multigrid methods.

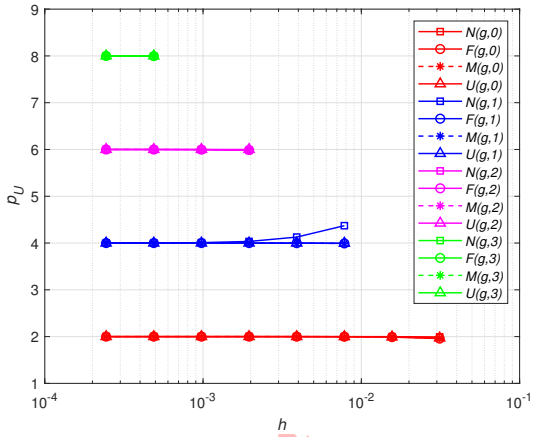

FIGURE 5. Apparent order (p_U) of discretization error for the variables N, F, M, and U.

TABLE 3. Effectiveness of the estimators $U_{\psi*}$ and U_{pmc} for the variables N, F, M and U.

h	Variable N		Variable F		Variable M		Variable U	
	$U_{\psi*}/E_m$	U_{pmc}/E_m	$U_{\psi*}/E_m$	U_{pmc}/E_m	$U_{\psi*}/E_m$	U_{pmc}/E_m	$U_{\psi*}/E_m$	U_{pmc}/E_m
6.25E-02	1.01716	1.01597	1.00731	0.99920	1.00516	0.99914	1.00488	0.99933
3.13E-02	0.95700	0.97161	0.98785	0.98707	0.98814	0.98730	1.00066	0.99999
1.56E-02	1.03044	1.00033	1.01460	1.00130	1.01400	1.00095	0.98688	0.98687
7.81E-03	0.97639	0.97671	0.99508	0.99637	0.99218	0.99311	1.00973	0.99634
3.91E-03	1.02560	1.00111	1.00504	1.00137	1.00821	1.00120	1.00500	1.00131
1.95E-03	0.99897	1.00008	0.99879	1.00015	0.99891	1.00011	0.99883	1.00013
9.77E-04	0.99946	0.99955	0.99973	0.99989	0.99961	0.99971	0.99969	0.99982
4.88E-04	1.00053	1.00007	1.00006	0.99995	1.00028	1.00000	1.01840	1.01821

As observed in Figure 5, when there is still no extrapolation ($m = 0$), p_U monotonically approaches the asymptotic order $p_A = 2$ as h is reduced. Therefore, the approximations of the tumor growth model solutions, resulting from the discretization of the differential equations, Eqs. (2.8), (2.9), (2.10), and (2.11), produce second-order methods ($p_0 = p_A = 2$), which is consistent with the literature [39, 45, 46]. Furthermore, it can be observed that for when there is extrapolation, and employing the RRE technique, the values of p_U converge to the sequences of the subsequent true orders, $p_1 = 4$, $p_2 = 6$ and $p_3 = 8$. According to Marchi et al. [25], the true orders follow an arithmetic sequence, and for additional levels of extrapolation, so they continue as $p_4 = 10$, and so on.

Another alternative way to verify the code is through the analysis of effectiveness of discretization error estimators. Table 3 presents the calculated effectiveness values $\theta(U)$ for the estimators U_{pmc} and $U_{\psi*}$. Both estimators demonstrate high accuracy with $\theta(U) \approx 1$. However, it is observed that U_{pmc} provides a more consistent approximation compared to $U_{\psi*}$. Therefore, U_{pmc} will be used to generate the graphs presented in Figure 6.

Figure 6 illustrates the results for the discretization error (E_h) and the Repeated Richardson extrapolation error (E_m) with their respective estimators U_{Ri} and U_{pmc}, considering all variables of the model.

When analyzing the discretization error E_h in Figure 6, it is clearly observable that the use of Repeated Richardson extrapolation, which generates E_m, is extremely effective in reducing this error across all variables. For example, in the case of variable N, shown in Figure 6(a), for $nm = 10$, which corresponds to $h = 4.8828125 \times 10^{-4}$, we have

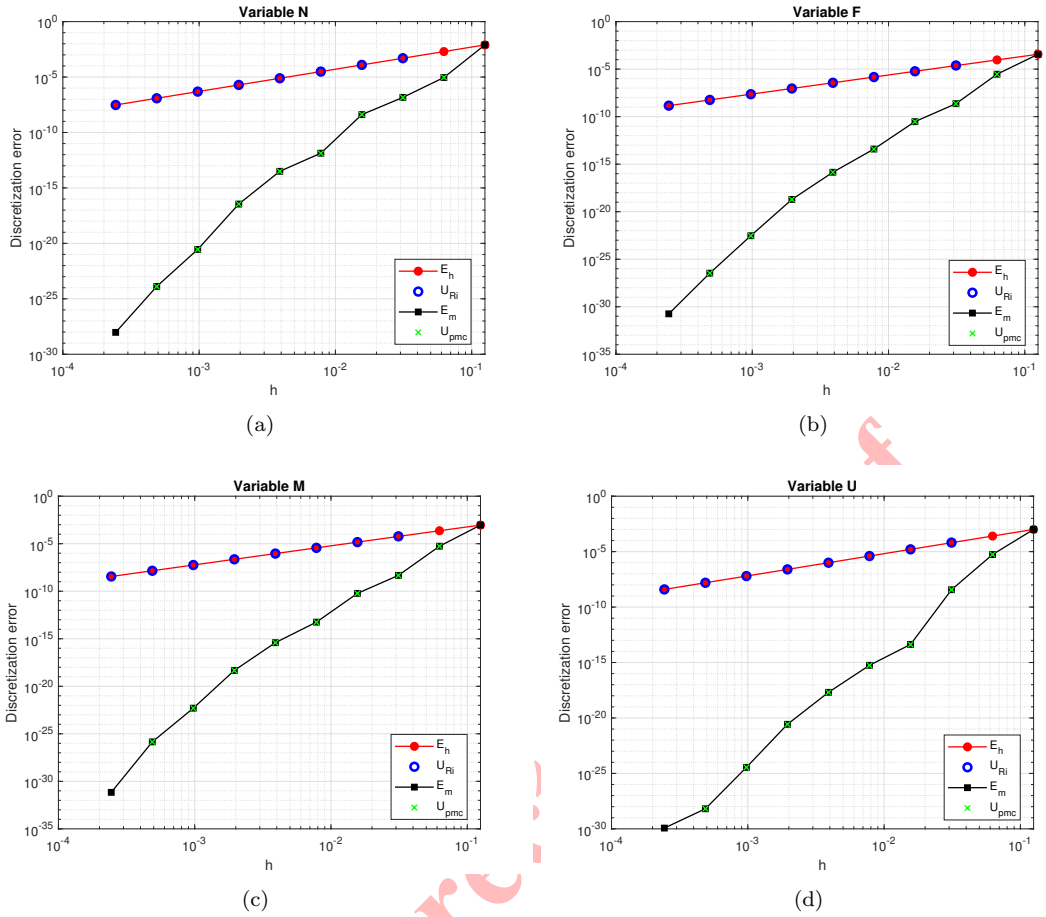

FIGURE 6. Discretization error without the use of the RRE (E_h), with its estimate (U_{Ri}), and with the use of the RRE (E_m) and its estimate (U_{pmc}) versus the spatial discretization h, considering the variables: (a) N, (b) F, (c) M, and (d) U.

$E_h \approx 10^{-7}$, while $E_m \approx 10^{-24}$. In summary, the application of RRE results in a significant reduction of the error E_m compared to E_h.

We can also observe in Figure 6, that both the estimator chosen for the discretization error without RRE (U_{Ri}), and with RRE (U_{pmc}), estimate well, making their use highly recommended in cases where the analytical solution is not known.

4.2. **Numerical test with a realistic problem.** In this section, we simulate a realistic problem using the model described by Eqs. (2.1)-(2.4), considering initial conditions that reflect the characteristics of a tumor for the variable n. Consequently, variables f, m and u are affected by this initial condition due to the coupling of the models. To evaluate the influence among the density of tumor cells n, extracellular matrix density f, matrix-degrading enzymes m and endogenous inhibitor u, we consider that interactions occur in an isolated system. Therefore, the boundary conditions are of Dirichlet type, given by

$$n(\mathbf{x_b}, t) = 0, \tag{4.13}$$

$$f(\mathbf{x_b}, t) = 1, \tag{4.14}$$

$$m(\mathbf{x_b}, t) = 0, \tag{4.15}$$
$$u(\mathbf{x_b}, t) = 0, \tag{4.16}$$

for $t > 0$, $\mathbf{x_b} \in \partial\Omega$, in which $\partial\Omega$ represents the boundary of the domain assumed.

Initially, we assume the presence of a tumor nodule in the domain $\Omega = [0, 1] \times [0, 1]$, with the initial tumor density centered at the point $(0.5, 0.5)$. This suggests that the tumor has already degraded some of the surrounding tissue in the assumed domain. The initial conditions are specified [21]

$$n(\mathbf{x}, 0) = exp\left(-\frac{c^2}{\epsilon} \right), \tag{4.17}$$
$$f(\mathbf{x}, 0) = 1 - 0.5n(x, y, 0), \tag{4.18}$$
$$m(\mathbf{x}, 0) = 0.5n(x, y, 0), \tag{4.19}$$
$$u(\mathbf{x}, 0) = 0, \tag{4.20}$$

where $\mathbf{x} = (x, y) \in \Omega$, c is defined by $c = \sqrt{(x - 0.5)^2 + (y - 0.5)^2}$ and $\epsilon = 0.01$, which corresponds to the density of cancerous cells.

Unlike the previous section, the problem addressed in this section does not have an analytical solution. To solve it, we considered the physical parameters presented in Table 1, adopting $\gamma = 10^{-3}$, $t_f = 5$ and employed a previously tested and verified multigrid code, which demonstrated high efficiency.

Figure 7 presents the estimate of discretization error without and with RRE, using the estimators U_{Ri} and U_{pmc} which were calibrated in Section 4.1. In both cases, the asymptotic order p_A was assumed. We can confirm from this same figure how the use of the RRE technique significantly reduced the discretization error for this problem, yielding accurate results. For example, in the variable N, Figure 7(a), for $nm = 10$, which corresponds to $h = 9.76562 \times 10^{-4}$, $E_h \approx 10^{-7}$, while $E_m \approx 10^{-15}$. Note that the variable F, Figure 7(b), exhibits an atypical behavior, which is justified by the problem modeling. The extracellular matrix (ECM) degrades rapidly, approaching zero at the central point. This causes the error estimate to be very small.

Although the primary objective of this work is the numerical verification of the proposed methodology, the computed solution also allows a qualitative assessment of the biological behavior reproduced by the model. Therefore, to illustrate the temporal evolution of the interacting variables, Figure 8 presents horizontal cross-sections through the center of the computational domain at selected time instants.

Figure 8(a) shows that the tumor cell density (N), initially concentrated near the center of the domain, gradually spreads over time, indicating the progression of the invasion process. Figure 8(b) shows the degradation of the extracellular matrix (F) in the regions occupied by tumor cells, resulting in a pronounced reduction of ECM density near the center of the domain. As shown in Figure 8(c), the concentration of matrix-degrading enzymes (M) increases in regions with higher tumor cell density, contributing to the degradation of the extracellular matrix. Finally, Figure 8(d) shows the accumulation of the endogenous inhibitor (U) over time, reflecting its interaction with the matrix-degrading enzymes.

Overall, the numerical results reproduce the qualitative behavior expected from the biological mechanisms incorporated into the mathematical model, providing additional confidence in the reliability of the proposed numerical methodology. Furthermore, the observed dynamics are consistent with results reported in the literature [18, 21, 22].

5. Conclusion

This study presented an efficient, robust, and accurate method for solving a two-dimensional avascular tumor growth model. Numerical tests with a known analytical solution and a realistic tumor growth model validated the proposed approach. The key results of the study are as follows:

- The multigrid method significantly reduced processing time compared to singlegrid, with a consistent average convergence factor close to zero, indicating high efficiency and robustness.
- The Richardson estimator (U_{Ri}) provided an excellent approximation of the discretization error for both analytical and realistic scenarios, ensuring reliable results.

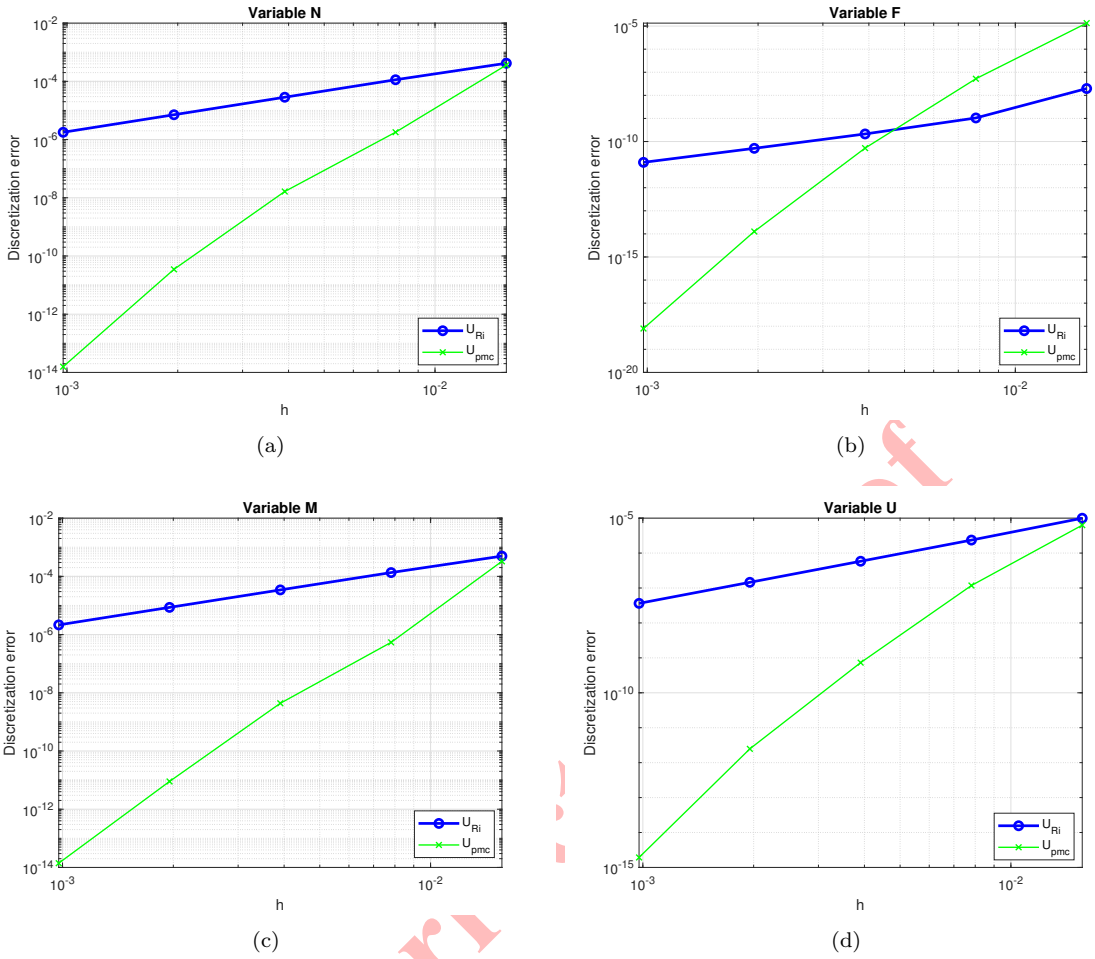

FIGURE 7. Estimate of the discretization error without using RRE (U_{Ri}) and estimate with RRE (U_{pmc}) versus the spatial discretization h for (a) N, (b) F, (c) M, and (d) U.

- The application of the Multiple Richardson Extrapolation (RRE) technique demonstrated a significant reduction in discretization error, achieving results with high precision and reliability.
- For cases with a known analytical solution, the U_{ψ^*} and U_{pmc} estimators were analyzed, with U_{pmc} recommended due to its superior precision. For the realistic problem, U_{pmc} was exclusively used, yielding satisfactory results.

These findings highlight the computational efficiency and accuracy of the proposed methodology, making it a promising tool for modeling complex biological systems. Future work will focus on applying the proposed framework to more detailed biological investigations of tumor growth, including the analysis of variable dynamics and parameter influence.

ACKNOWLEDGMENT

This work was supported by Coordenação de Aperfeiçoamento de Pessoal de Nível Superior (CAPES), Brazil – Finance Code 001.

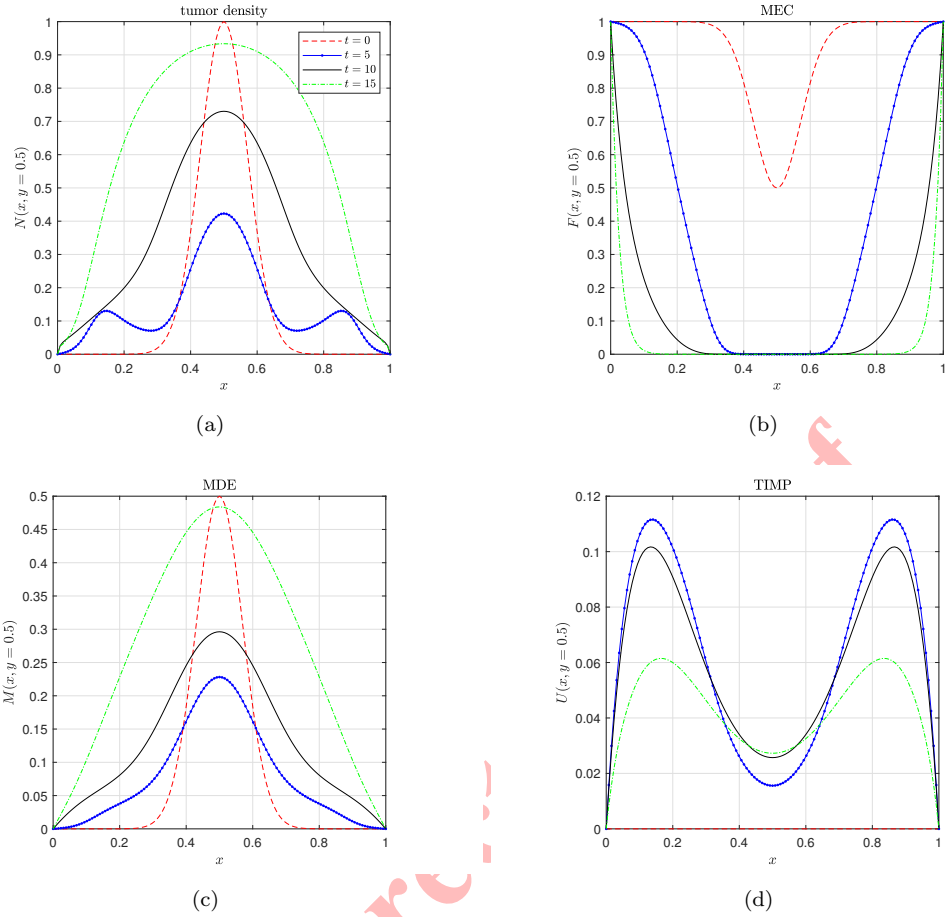

FIGURE 8. Horizontal cross-sections through the center of the computational domain at $t = 0$, 5, 10, and 15 for (a) tumor cell density (N), (b) extracellular matrix density (F), (c) matrix-degrading enzyme concentration (M), and (d) endogenous inhibitor concentration (U).

REFERENCES

[1] M. A. Aba Oud, A. Ali, H. Alrabaiah, S. Ullah, M. A. Khan, and S. Islam, *A fractional order mathematical model for COVID-19 dynamics with quarantine, isolation, and environmental viral load*, Adv. Differ. Equ., *2021* (2021), 1–19.

[2] H. K. I. Al-Mahdawi, M. Abotaleb, H. Alkattan, A.-M. Z. Tareq, A. Badr, and A. Kadi, *Multigrid method for solving inverse problems for heat equation*, Mathematics, *10* (2022), 2802.

[3] A. R. A. Anderson, M. A. J. Chaplain, E. L. Newman, R. J. C. Steele, and A. M. Thompson, *Mathematical modelling of tumour invasion and metastasis*, Comput. Math. Methods Med., *2* (2000), 129–154.

[4] E. O. Belinelli, L. H. Fantin, M. G. Canteri, K. Braga, E. R. Cirilo, N. M. L. Romeiro, and P. L. Natti, *Numerical simulation of atmospheric transport of Phakopsora pachyrhizi urediniospores in South America using the state of Paraná-Brazil as a model*, Eur. J. Plant Pathol., *163* (2022), 979–990.

[5] W. L. Briggs, V. E. Henson, and S. F. McCormick, *A Multigrid Tutorial*, 2nd ed., SIAM, Philadelphia, 2000.

[6] R. L. Burden, J. D. Faires, and A. M. Burden, *Análise Numérica*, 3ª ed. brasileira, Cengage Learning, São Paulo, 2016.

[7] C. G. Cess and S. D. Finley, *Calibrating agent-based models to tumor images using representation learning*, PLOS Comput. Biol., *19* (2023), e1011070.

[8] M. A. J. Chaplain and A. R. A. Anderson, *Mathematical modelling of tissue invasion*, in *Cancer Modelling and Simulation*, L. Preziosi (Ed.), Chapman & Hall/CRC, Boca Raton, 2003, 269–297.

[9] M. A. J. Chaplain and G. Lolas, *Mathematical modelling of cancer cell invasion of tissue: the role of the urokinase plasminogen activation system*, Math. Models Methods Appl. Sci., *15* (2005), 1685–1734.

[10] J. A. Cuminato and M. Meneguette, *Discretização de Equações Diferenciais Parciais: Técnicas de Diferenças Finitas*, Sociedade Brasileira de Matemática, Rio de Janeiro, 2013.

[11] G. Dahlquist and Å. Björck, *Numerical Methods in Scientific Computing*, SIAM, Philadelphia, 2008.

[12] S. Evje, *An integrative multiphase model for cancer cell migration under influence of physical cues from the microenvironment*, Chem. Eng. Sci., *165* (2017), 240–259.

[13] R. P. Fedorenko, *The speed of convergence of one iterative process*, USSR Comput. Math. Math. Phys., *4* (1964), 227–235.

[14] A. C. Foltran, C. H. Marchi, and L. M. Moura, *Verification of numerical solutions of thermal radiation problems in participating and nonparticipating media*, Numer. Heat Transfer Part B Fundam., *84* (2023), 143–165.

[15] A. de O. Fortuna, *Técnicas Computacionais para Dinâmica dos Fluidos: Conceitos Básicos e Aplicações*, Edusp, São Paulo, 2000.

[16] G. R. Gandhi, C. S. Sharanya, A. Jayanandan, M. Haridas, V. E. Hillary, S. R. Gandhi, G. Sridharan, R. Sivasubramanian, A. B. Silva Vasconcelos, M. M. Montalvão, et al., *Multitargeted molecular docking and dynamics simulation studies of flavonoids and volatile components from the peel of* Citrus sinensis *L. (Osbeck) against specific tumor protein markers*, J. Biomol. Struct. Dyn., *42* (2024), 3051–3080.

[17] N. Habibi, A. Mesforush, F. J. Gaspar, and C. Rodrigo, *Semi-algebraic mode analysis for finite element discretisations of the heat equation*, Comput. Methods Differ. Equ., *9* (2021), 146–158.

[18] M. Kolev and B. Zubik-Kowal, *Numerical solutions for a model of tissue invasion and migration of tumour cells*, Comput. Math. Methods Med., *2011* (2011), Article ID 452320, 16 pages.

[19] A. Kumar, *Study and analysis of different segmentation methods for brain tumor MRI application*, Multimed. Tools Appl., *82* (2023), 7117–7139.

[20] G. Leduc, *The Boyle–Romberg trinomial tree, a highly efficient method for double barrier option pricing*, Mathematics, *12* (2024), 964.

[21] L. G. López, C. A. Ruiz, and A. P. Castaño, *Numerical simulation of tumor growth and cell migration in 1D and 2D*, Revista Argentina de Bioingeniería, *22* (2018), 60–66.

[22] J. Maganin, N. M. L. Romeiro, E. R. Cirilo, and P. L. Natti, *Simulation of a mathematical model of tumoral growth using finite differences*, Braz. J. Dev., *6* (2020), 87696–87709.

[23] M. F. Malacarne, M. A. V. Pinto, and S. R. Franco, *Performance of the multigrid method with time-stepping to solve 1D and 2D wave equations*, Int. J. Comput. Methods Eng. Sci. Mech., *23* (2022), 45–56.

[24] C. H. Marchi and A. F. C. Silva, *Unidimensional numerical solution error estimation for convergent apparent order*, Numer. Heat Transfer Part B Fundam., *42* (2002), 167–188.

[25] C. H. Marchi, M. A. Martins, L. A. Novak, L. K. Araki, M. A. V. Pinto, S. F. T. Gonçalves, D. F. Moro, and I. S. Freitas, *Polynomial interpolation with repeated Richardson extrapolation to reduce discretization error in CFD*, Appl. Math. Model., *40* (2016), 8872–8885.

[26] C. H. Marchi, C. D. Santiago, and C. A. R. Carvalho Jr., *Lid-driven square cavity flow: A benchmark solution with an 8192 × 8192 grid*, J. Verif. Valid. Uncert. Quantif., *6* (2021), 041005.

[27] F. E. Merga and H. M. Chemeda, *Modified Crank–Nicolson scheme with Richardson extrapolation for one-dimensional heat equation*, Iran J. Sci. Technol. Trans. A Sci., *45* (2021), 1725–1734.

[28] M. Ramezani, R. Mokhtari, and G. Haase, *A multigrid solver for subdiffusion equations*, Comput. Methods Differ. Equ., 2025, 1–16.

[29] C. F. Ng and H. B. Frieboes, *Simulation of multispecies desmoplastic cancer growth via a fully adaptive non-linear full multigrid algorithm*, Front. Physiol., *9* (2018), 821.

[30] W. L. Oberkampf and F. G. Blottner, *Issues in computational fluid dynamics code verification and validation*, AIAA J., *36* (1998), 687–695.
[31] M. L. de Oliveira, M. A. V. Pinto, C. Rodrigo, and F. J. Gaspar, *Modified Picard with multigrid method for two-phase flow problems in rigid porous media*, Int. J. Numer. Methods Eng., *125* (2024), e7397.
[32] M. A. V. Pinto, C. Rodrigo, F. J. Gaspar, and C. W. Oosterlee, *On the robustness of ILU smoothers on triangular grids*, Appl. Numer. Math., *106* (2016), 37–52.
[33] R. H. Pletcher, J. C. Tannehill, and D. Anderson, *Computational Fluid Mechanics and Heat Transfer*, 3rd ed., CRC Press, Boca Raton, 2012.
[34] D. Rigoni, M. A. V. Pinto, and J. E. Kwiatkowski Jr., *Verification and error analysis for the simulation of the grain mass aeration process using the method of manufactured solutions*, Biosyst. Eng., *223* (2022), 149–160.
[35] D. Rigoni, M. A. V. Pinto, and J. E. Kwiatkowski Jr., *On space–time ratio in the soybean mass aeration problem using a manufactured solution with realistic parameters*, Comput. Electron. Agric., *214* (2023), 108300.
[36] Á. P. de la Riva, C. Rodrigo, F. J. Gaspar, J. H. Adler, X. Hu, and L. Zikatanov, *A local Fourier analysis for additive Schwarz smoothers*, Comput. Math. Appl., *158* (2024), 13–20.
[37] P. J. Roache, *Fundamentals of Computational Fluid Dynamics*, Hermosa Publishers, Albuquerque, NM, 1998.
[38] P. J. Roache and P. M. Knupp, *Completed Richardson extrapolation*, Commun. Numer. Methods Eng., *9* (1993), 365–374.
[39] S. Rodrigues, M. A. V. Pinto, M. A. Martins, and S. R. Franco, *Reducing the discretization error for a poroelasticity problem in variables having extreme values*, J. Braz. Soc. Mech. Sci. Eng., *44* (2022), 162.
[40] C. J. Roy, *Review of code and solution verification procedures for computational simulation*, J. Comput. Phys., *205* (2005), 131–156.
[41] P. Roy, N. Anand, and D. Donzis, *A parallel multigrid finite-volume solver on a collocated grid for incompressible Navier–Stokes equations*, Numer. Heat Transfer Part B Fundam., *67* (2015), 376–409.
[42] S. S. Sajjadi, D. Baleanu, A. Jajarmi, and H. M. Pirouz, *A new adaptive synchronization and hyperchaos control of a biological snap oscillator*, Chaos Solitons Fractals, *138* (2020), 109919.
[43] C. D. Santiago, G. R. Ströher, M. A. V. Pinto, and S. R. Franco, *A multigrid Waveform Relaxation Method for solving the Pennes bioheat equation*, Numer. Heat Transfer Part A Appl., *83* (2023), 976–990.
[44] T. W. H. Sheu and R. K. Lin, *Newton linearization of the incompressible Navier–Stokes equations*, Int. J. Numer. Methods Fluids, *44* (2004), 297–312.
[45] L. P. da Silva, B. B. Rutyna, A. R. S. Righi, and M. A. V. Pinto, *High Order of Accuracy for Poisson Equation Obtained by Grouping of Repeated Richardson Extrapolation with Fourth Order Schemes*, Comput. Model. Eng. Sci., *128* (2021), 699–715.
[46] L. P. da Silva, C. H. Marchi, M. Meneguette, and A. C. Foltran, *Robust RRE technique for increasing the order of accuracy of SPH numerical solutions*, Math. Comput. Simul., *199* (2022), 231–252.
[47] S. Tanwar, L. Famhawite, and P. R. Verma, *Numerical simulation of bio-heat transfer for cryoablation of regularly shaped tumours in liver tissue using multiprobes*, J. Therm. Biol., *113* (2023), 103531.
[48] K. Tiwari et al., *Reproducibility in systems biology modelling*, Mol. Syst. Biol., *17* (2021), e9982.
[49] U. Trottenberg, C. W. Oosterlee, and A. Schüller, *Multigrid*, Academic Press, San Diego, 2001.
[50] S. M. Wise, J. S. Lowengrub, H. B. Frieboes, and V. Cristini, *Three-dimensional multispecies nonlinear tumor growth–I: model and numerical method*, J. Theor. Biol., *253* (2008), 524–543.
[51] S. M. Wise, J. S. Lowengrub, and V. Cristini, *An adaptive multigrid algorithm for simulating solid tumor growth using mixture models*, Math. Comput. Model., *53* (2011), 1–20.
[52] P. D. Zen, M. A. V. Pinto, and S. R. Franco, *A multigrid waveform relaxation method for solving the nonlinear silicon problem with relaxing boundary conditions*, Numer. Heat Transfer Part B Fundam., 2024, 1–16.
[53] J. Z. Zhu and O. C. Zienkiewicz, *Superconvergence recovery technique and a posteriori error estimators*, Int. J. Numer. Methods Eng., *30* (1990), 1321–1339.